Submitted to ADVANCED MATERIALS

DOI: 10.1002/((please add manuscript number))
Article type: Communication

Atomic vacancies control of Pd-based catalysts for enhanced electrochemical performance

*Yunpeng Zuo[†a], Dewei Rao[†b], Shuo Li[a], Tingting Li[d], Guilin Zhu[a], Shuangming Chen[e], Li Song[e], Yang Chai[*c], Heyou Han[*a]*

Y. Zuo, S. Li, G. Zhu, Prof. H. Han

[a]State Key Laboratory of Agricultural Microbiology, College of Science, Huazhong Agricultural University, Wuhan 430070, P R China.

E-mail: hyhan@mail.hzau.edu.cn.

Dr. D. Rao

[b]School of Materials Science and Engineering, Jiangsu University, Zhenjiang 212013, P R China.

Dr. T. Li

[d]Key Laboratory of Micro-Nano Materials for Energy Storage and Conversion of Henan Province, Institute of Surface Micro and Nano Materials, Xuchang University, Xuchang, Henan 461002, P R China.

Y. Zuo, Prof. Chai

[c]Department of Applied Physics, The Hong Kong Polytechnic University, Hung Hom, Kowloon, Hong Kong, P R China.

E-mail: ychai@polyu.edu.hk.

Dr. S. Chen, Prof. L. Song

[e]National Synchrotron Radiation Laboratory, CAS Center for Excellence in Nanoscience, University of Science and Technology of China, Hefei, Anhui 230029, P R China.

Keywords: PdCuCo alloys, exterior atomic vacancy, compressive strain, oxygen reduction reaction, enhanced electrochemical performance

Abstract: Structure-engineered Pd-based catalysts at atomic level can effectively improve the catalytic performance for the oxygen or small organic molecules electrocatalysis, comparable to or even superior to that of commercial Pt/C. Here we synthesized PdCuCo anisotropic structure (AS) electrocatalysts with abundant vacancy defects on the exterior surface, which is unambiguously verified by aberration-corrected transmission electron microscopy. The

PdCuCo-AS with vacancy (v-PdCuCo-AS) show excellent electrochemical activity towards oxygen reduction reaction (ORR) and oxidation of alcohols. The mass activity (MA) of the v-PdCuCo-AS is 0.18 A/mg at 0.9 V vs. RHE, which is 15.55 times larger than that of the commercial Pd/C catalyst in acidic electrolyte. According to our theoretical calculations, this significant improvement can be understood as a result of the promoted charge transfer by polarized electronic structures of the v-PdCuCo-AS in the processes of ORR. The synergistic effect of the correlated defects, the compressive strain caused by the doping Co and Cu atoms effectively improve the electro-catalysis activity for the ORR in acidic/alkaline electrolyte on the v-PdCuCo-AS stems. This approach provides a strategy to design other AS structures for improving their electrochemical performance.

Controlling the exterior surface structure of the electrode materials can be used to enhance the activity of catalyst, which has been widely applied for the sustainable conversion processes of water-hydrogen-oxygen, including the oxygen reduction reaction (ORR), oxygen evolution reaction (OER) and hydrogen evolution reaction (HER).[1-5] The configuration of surface electronic structure is closely related to the arrangement of surface atoms of the materials.[6-9] However, most current systems only focuse on the structures, sizes or components, neglecting the effect of the intrinsic defects of the crystals.[1, 10-13] In fact, it is quite difficult to obtain the catalysts without defects.[4] Some studies have demonstrated that the catalysts with defects on the surface possess higher activity than the defect-free ones.[4,16] For instance, it has been proved that the activity of the edge carbon is higher than basal plane carbon for the ORR.[17] Meanwhile, S-vacancies in the basal plane of MoS_2 provide more exposed Mo atoms to directly bind with hydrogen.[18] The catalysts with controllable defects have great potential for high activity and the commercialization of the noble metal catalysts.

Fuel cells are high-efficiency energy-conversion devices.[19-23] The best currently known electro-catalysts for ORR and liquid fuels-oxidation reaction are the Pt-based catalysts, which suffers from high cost, undesirable durability and low CO poisoning tolerance problems.[23] Recently, Pd-based catalysts have been demonstrated to be promising effective catalysts because of their outstanding activities for ORR and electrochemical oxidation of small organic molecules, which show potential alternatives for the Pt-based catalysts.[13, 24-26] Previous studies show appreciable enhancement of the activity of the catalysts in water-splitting and fuel cells by alloying Pd with the transition metals, exposing the low-coordinated surface atoms and altering the distances between surface atoms to control the defect or strain of catalysts.[13,26-28] A range of transition metals, including Fe, Co and Ni, have been intensively explored into PdCu active bimetallic system by simultaneously decreasing material cost and enhancing performance.[4,22,23] The specific activity for ORR of the ordered PdCuCo nanoparticles can reach 1.3 times higher than that of commercial Pt/C with the

compressive strain on the surface of the catalysts.[13] Huang and his co-workers found that the ascorbic acid (AA) not only acts as the reductant, but also works as the weak acid to remove the heteroatoms, forming the pure Pt phase on the surface of the crystals.[29] Thus the heteroatoms can be synchronously and selectively removed in the reaction to obtain the catalysts with abundant defects. Stimulated by this, considerable efforts have been made to develop the PdCuCo catalysts with abundant vacancies (v-PdCuCo) towards oxygen electrocatalysis.

In this work, we show a general method with high reproducibility for controllable synthesis of a class of multicomponent anisotropic structure (AS) with abundant active defect sites. The open AS addresses large specific surface area, 3D surface molecular accessibility and high densities of corners, edges and stepped atoms, which can optimize the use of noble metals.[6,30,31] The structural characterization analysis was obtained by aberration corrected high resolution transmission electron microscopy (HRTEM), indicating the existence of atomic vacancies. The anisotropic materials can achieve high surface-to-volume ratio even though there is an accumulation of the carbon-supported catalyst. Our density functional theory (DFT) calculations reveal that the vacancies enable the polarization of surface electronic structure for v-PdCuCo-AS, which can improve the ORR activities of the v-PdCuCo-AS. Moreover, up-scaled synthesis of v-PdCuCo-AS can be readily achieved at gram scale, and the approach is an effective strategy to design other AS systems.

The structures of as-prepared v-PdCuCo-AS are characterized by aberration-corrected transmission electron microscopy (AC-TEM). **Figure 1**A shows representative high angle annular dark field (HAADF) images of v-PdCuCo-AS. The geometry of multi-hierarchical structure (Figure 1A, S1) with the branch diameter of ~9 nm is observed, which can help the molecular to contact with catalysts.[6,30] The selected-area electron diffraction (SAED) of the as-prepared nanomaterials (inset of Figure 1A) shows the v-PdCuCo-AS is single crystalline, with the corresponding diffraction pattern from the [02-2] zone axis of PdCu cubic

phase.[13,32,33] The obvious contrast between the vacancies sites and bulk atoms can be attributed to the ingredients in the v-PdCuCo-AS. A typical area of v-PdCuCo-AS image (Figure 1B) was selected to observe the dispersed vacancies sites. The enlarged HRTEM images show the atomic structure of v-PdCuCo-AS with the [110] direction in the zone axis. As a rigorous technique to document the element distribution of the nanomaterials, STEM-EDS elemental mapping of the individual v-PdCuCo-AS shows that Co is homogeneously distributed in the interior area of the catalyst, whereas Pd and Cu were distributed throughout the v-PdCuCo-AS structure (Figure 1C, S2). The outer heteroatoms might be etched by AA owing to the weak acid.[29] The HRTEM images of v-PdCuCo-AS clearly show the vacancies sites are uniformly distributed around the catalysts (Figure $1B_{1,2}$). The higher magnification HRTEM and the inset HAADF images in Figure $1B_{1,2}$ indicated the vacancies, which can be identified from their different contrast as the red arrows indicate. These results are further supported by the XRD and TEM-EDS. It is noteworthy that there are no typical diffraction peaks of Cu or its oxides, and the peaks are in the central area between the fcc Pd and Cu, indicating the formation of PdCu alloy.[13,32,33] From the XRD spectrum (Figure 1D), the diffraction peaks can be well identified to the (111), (200), (220), and (311) for the fcc PdCu-AS with the JCPDS number: 48-1551. The XRD pattern of v-PdCuCo-AS significantly shifts to low angle x-ray diffraction area owing to the increased lattice spacing by imbedding Co atoms.[34,35]

Surface analysis of the v-PdCuCo-AS was carried out using X-ray photoelectron spectroscopy (XPS) technique (Figure S3). The XPS spectroscopy shows the presence of Pd, Cu, and Co in the catalyst. The presence of the blurry Co peak in the full spectrum (Figure S3A) and the enlarged single unsharp Co2p peak in Figure S3B reveal that the surface Co atoms were leached away from the PdCuCo catalysts,[36-38] in consistent with the STEM EDS-mapping-based study of v-PdCuCo-AS catalysts. The X-ray absorption near edge structure (XANES) and extended x-ray absorption fine structure (EXAFS) in Figure S4 show

negligible change of Cu for the PdCu-AS and v-PdCuCo-AS catalysts, which reveal the vacancy defects on the surface of the v-PdCuCo-AS are caused by removing of Co atoms as mentioned before. The compositional ratio between Pd/Cu/Co is 3.87/1/0.01 for the v-PdCuCo-AS, as revealed by ICP-MS documented in Table S1. The ICP-MS results confirmed the low Co content as revealed by STEM-EDS mapping. The vacant sites might be influenced by the use of AA, which can act as a weak acid for removing the heteroatoms, allowing the abundant vacancies sites to diffuse on the exterior surface of the v-PdCuCo-AS.[29,37]

We can observe that abundant vacancies sites with randomly scattered distribution over the surface through the HRTEM image obtained from the [100] axis in **Figure 2**A. The corresponding HAADF images in the Figure 2B and 2C reveal that the defective regions (pointed out by the red arrow) mainly exist on the surface of the v-PdCuCo-AS structure, which provide further evidence for the results shown in Figure 1. For the fcc PdCu nanocrystals, the atomic arrangement forms alternating packing of Pd and Cu atoms along the <100> direction. While for the v-PdCuCo-AS, the Co atoms possibly cause the polar facets owing to embedded configuration and the intrinsic physical property. There is a significant difference of the arrangement of the crystal structure between the PdCu-AS and v-PdCuCo-AS (comparing the Figure 2A and 2B with Figure 2D, Figure S5). Figure 2E and F show the approximate PdCu and v-PdCuCo-AS crystal structures along the [100] direction with Pd in grayness, where Cu is in blue and Co is in soft blue. For the PdCu-AS, the adjacent Pd-Cu and Cu-Cu atom–atom distances are 2.704 and 2.628 Å (Figure 2E), however, the adjacent Cu-Pd atom–atom distance decreases to 2.675 Å with the increase of Cu-Pd atom–atom distance after embedded Co atoms to the PdCu crystal. To further identify the atomic arrangement of the surface structure, the approximate v-PdCuCo-AS crystal structure from [232] and [100] perspectives (Figure 2G, H) are helpful for understanding the distinction of the different metal atoms in the bulk catalyst. The vacancies on the surface possess slightly larger atomic distances than the inner Pd atoms do, which provides spatial locations for strain

release.[39] The approximate v-PdCuCo-AS crystal structures in Figure 2G and H show that the coordination number of the surface atoms are undercoordinated relative to typical crystal surfaces.[40] For the PdCuCo catalyst, the surface charge density at site of Co is changed as the formation of vacancy (Figure 2I, 2J and S6). It is noteworthy that the introduction of Co can also increase the electronic polarization of the PdCu-AS (Figure 2I and S6), which helps to overcome the reaction barrier of the limiting steps of ORR, thus improving ORR activity.[41]

The formation process of v-PdCuCo-AS contains nucleation and growth steps. [2d, 22] The CTAB molecules and Br^- act as the capping agents, which have great effect on the final structure of the v-PdCuCo-AS materials.[42] The metal atoms agglomerate to form nanoclusters, which subsequently grow to small PdCuCo particles (Figure S7A and S7B) after the content of corresponding atoms reached the level of supersaturation.[42] The formation of small PdCuCo particles may abide by the law of Wulff's theorem, attempting to minimize the total interfacial free energy (γ) of the system.[43-47] This result is consistent with the previously reported papers on the shape evolution of the nanocrystals.[42-47] The reaction progress of PdCuCo truncated nanocubic generated from the PdCuCo particles is shown in Figure S7A and S7C. The new generated zero-valent metal atoms deposit onto the special active sites as the CTAB molecules and Br^- absorb on the {100} facets, which have remarkable influence on the surface energy.[9, 43-47] The differentiation of the interfacial energy for the intermediates accelerates the island growth to form the anisotropic structures, as shown in Figure S7A and S7D. There are abundant steps, corners on the surface of the catalyst in the formation of the branches, which comprise the high-index facets {310}, {420} in the inset HRTEM images (Figure S7A). According to enlarged HRTEM images in Figure S7A, the lattice spacing of the architecture is estimated to be 0.22 nm (Figure S7A), consistent with the {111} facets of *fcc* PdCuCo crystal, confirming the growth of PdCuCo branch at <111> direction and the existence of PdCuCo nanocubics. After the PdCuCo-AS generation, the composites continue

to stir for a period of time to leach away the Co or Cu atoms on the surface to generate the vacancies sites for the v-PdCuCo-AS.

The electrochemical performance of the PdCu-AS and v-PdCuCo-AS towards ORR were evaluated in O_2-saturated 0.1 M $HClO_4$ solution against the commercial Pd/C (20% Pd, JM) (**Figure 3**). The electro-chemical surface area (ECSA) of the catalysts were determined by integrating the hydrogen adsorption charge on cyclic voltammograms (CVs), as shown in Figure 3A. The characteristic region of Hupd ($H^+ + e^- = Hupd$) adsorption/desorption for the Pd/C, PdCu-AS and v-PdCuCo-AS is in the potential range from 0.05 to 0.4 V. The reduction of Pd oxide for the OHad ($2H_2O = OHad + H_3O^+ + e^-$) is in the potential between 0.65 and 1.25 V. The ECSA/g_{Pd} of the Pd/C, PdCu-AS and v-PdCuCo-AS are 41.79, 72.18 and 70.46 m^2/g, respectively. That is mainly because the AS can offer the 3D surface molecular accessibility. [6] The reduction potential of surface oxides of the PdCu-AS and v-PdCuCo-AS shift positively by 102 and 116 mV compared to Pd/C, revealing the decrease in oxygen affinity of the PdCu-AS and v-PdCuCo-AS.[48] The ORR polarization curves normalized with respect to the area of glassy carbon electrode (0.196 cm^2) are presented in Figure 3B. The half-wave potential for v-PdCuCo-AS is 0.915 V vs.RHE, which is obviously higher than that of the commercial Pd/C (0.856 V vs.RHE) and PdCu-AS (0.88 V vs.RHE) as shown in Figure 3B, suggesting significantly enhanced ORR activity for v-PdCuCo-AS catalyst.[40] The kinetic currents are calculated in accordance with the Koutecky-Levich equation.[40,41,49-51] As seen from the corresponding Tafel plots in Figure 3B, v-PdCuCo-AS exhibits significantly improved kinetics with a smaller slope compared with PdCu-AS, revealing that the randomly distributed defective sites can effectively improve the activity of the v-PdCuCo-AS.[40,41,48] To better assess the ORR activity, we also analyze the corresponding specific activity (SA) and mass activity (MA) of synthetic catalysts at 0.8 V and 0.9 V vs. RHE. Overall, as expected, the SA of v-PdCuCo-AS catalyst at 0.8 V vs. RHE

could reach 1.61 mA/cm^2, 2.4 times the SA of PdCu-AS (0.675 mA/cm^2) and 5.96 times the SA of Pd/C (0.27 mA/cm^2) (Figure 3C). The MA of v-PdCuCo-AS catalyst at 0.8 V vs. RHE is 1.135 A/mg, 10.67 and 2.33 times greater than those of the Pd/C (0.106 A/mg) and PdCu-AS (0.487 A/mg), respectively. Simultaneously, the SA of v-PdCuCo-AS catalyst at 0.9 V vs. RHE was 0.252 mA/cm^2, 3.42 times the SA of PdCu-AS (0.074 mA/cm^2) and 8.69 times of Pd/C (0.029 mA/cm^2) (Figure 3D), respectively. The MA of v-PdCuCo-AS catalyst at 0.9 V vs. RHE is 0.178 A/mg, 15.55 times the MA of the Pd/C (0.011 A/mg) and 3.34 times the MA of the PdCu-AS (0.053 A/mg) respectively. In addition, the electrocatalysis activity of commercial Pt/C was also tested to compare the performance with the v-PdCuCo-AS. The MA of the Pt/C at 0.9 V vs. RHE (0.1495 A/mg, Figure S8) is smaller than that of v-PdCuCo-AS (0.178 A/mg), which shows good catalytic performance of v-PdCuCo-AS. These results and the comparisons to Pd-based catalysts from recent studies in table S3 suggest an excellent structure and composition of the synthetic v-PdCuCo-AS. We also synthesized PdCuCo nanomaterials with different sizes, which contains the PdCuCo-AS (40 nm) and PdCuCo nanoparticles (20 nm), as shown in Figure S9. When the whole size of the dendritic structure reduces to 40 nm, the extension of the branched protuberance is also reduced (Figure S9A). The ORR polarization curves show that the catalytic activity of the PdCuCo-AS gradually decrease as the branched protuberance gets smaller (Figure S9B, S10). That mainly because of the branches in the PdCuCo-AS could adequate expose the active sites with the high densities of edges, corners, and stepped atoms[13b, 25]. We also applied the Pd-based electrocatalysts to the HER (Figure S11, 12 and Table S3). The v-PdCuCo-AS shows the better HER activity than PdCu-AS and commercial Pd/C, which further evidents the beneficial effects of the surface vacancies[6].

The accelerated degradation tests (ADT) of the v-PdCuCo-AS catalyst was tested in 0.1 M $HClO_4$ solution at the potential between 0.6 and 1.1 V (vs. RHE). Figure S13 shows the electrocatalytic durability of high-performance PdCu-AS and v-PdCuCo-AS catalysts. The

CVs, ORR polarization curves and the corresponding Tafel plots (Figure S13) of the PdCu-AS and v-PdCuCo-AS catalysts before and after 4000 cycles between 0.6 and 1.1 V vs. RHE. These results suggest good stability of the v-PdCuCo-AS. There is 13.36% loss of MA for the PdCu-AS at 0.9 V vs. RHE after 4000 cycles, while only 0.26 % loss of MA for the v-PdCuCo-AS under the same condition (Figure S14), revealing that the superior catalytic durability of the v-PdCuCo-AS catalyst. The catalytic performance variation between the PdCu-AS and v-PdCuCo-AS is likely to be caused by the synergistic effect of correlated defects and doped Co atoms. The compressive surface strain of the v-PdCuCo-AS protected the interior Pd atoms from losing by the place-exchange mechanism during the ADT. In addition, the self-supporting property of the special AS structure can improve the electro-catalysis stability of the v-PdCuCo-AS (Figure S13 and S14).[13,40] The structures of the v-PdCuCo-AS catalysts before and after ADT were characterized by HRTEM (Figure S15), showing negligible change of the structure.

The ORR polarization of the catalysts were also tested in O_2-saturated 0.1 M KOH solution as shown in Figure S16. The half-wave potentials of the v-PdCuCo-AS is 0.901 V, which is ~ 37 mV larger than that of PdCu-AS (0.864 V), suggesting its decreased ORR overpotential.[29] The corresponding Tafel plots inserted in Figure S16A further indicate the enhanced activity. At 0.8 V vs. RHE, the MA of the v-PdCuCo-AS is 0.21 A/mg, 1.63 times of PdCu-AS. Similar behavior is also observed at 0.9 V. The MA of the v-PdCuCo-AS is 1.68 times larger than that of PdCu-AS. The v-PdCuCo-AS reported herein also show excellent catalytic performance toward alcohol oxidation in half cells, such as methanol oxidation reaction (MOR) and ethanol oxidation reaction (EOR). As shown in Figure S16C and 16D, the v-PdCuCo-AS exhibits better MOR activity and shows 2.21 times MOR MA (0.17 A/mgPd) than PdCu-AS. For EOR, the MA of v-PdCuCo-AS is 0.823 A/mgPd (Figure S16E and 16F), 2.44 times higher than that of the PdCu-AS. Furthermore,

the two typical current peak ratios for the MOR and EOR, one on the forward (If) and the other on the reverse potential scan(Ib), can act as the preliminary evaluation for the anti-poisoning ability.[7,13] The ratio of If/Ib of the v-PdCuCo-AS for EOR is higher than that of PdCu-AS. Figure S17 shows the anodic portions of the CV corresponding to the CO oxidation process for the PdCu-AS and v-PdCuCo-AS. The onset potential of CO-stripping on v-PdCuCo-AS shifts more negatively than that on PdCu-AS, which further indicated that the v-PdCuCo-AS have a higher durability against CO poison than PdCu-AS.[52] The potential-dependent steady-state current curves (recorded at 3000 s) of EOR pointing toward the same trend is shown in Figure S18. The v-PdCuCo-AS for MOR exhibits inferior stability in the initial test, while conserves stability without obvious decay during subsequent tests. Apparently, v-PdCuCo-AS shows more superior stability compared to PdCu-AS. These results reveal that the catalysts with vacancies have better performance for MOR and EOR than the corresponding counterparts as illustrated in Table S4 and S5.

As widely accepted, modifying the electronic structure of the electrocatalysts through the control of defects is an intrinsic regulatory approach to improve its catalytic performance.[1d] For this system, the vacancies on the exterior surfaces of the catalyst play an important role in promoting the ORR performance of the v-PdCuCo-AS. To gain further insight on the relationship between the vacancies and ORR performance of the PdCuCo-AS, DFT calculations were performed to explore electronic structures of catalysts and their influence on catalytic properties. Clearly, the electrons are re-distributed around the vacancy on the surface of v-PdCuCo-AS, as shown in Figure 4A. Although the O_2 can maintain its construction above vacancy, but the bond distance of O_2 is expanded from 1.21 Å to 1.43 Å. These phenomena can be reasonably explained according to the charge transfer. As displayed in Figure 4B, some charge accumulation around O atoms and charge depletion areas in red colors can be found around Pd atoms, which means that the charge transferred from Pd atoms to O atoms, resulting in the ionization of O_2. The ionized O_2 can further enhance the

performance of ORR, in consistent with our experiment descriptions. Significantly, there is unobvious electron transfer from Cu to O_2, which means that the influence of Cu is limited in ORR. It has been experimentally demonstrated that the lattice of PdCu-AS is expanded for Co-embedding, and the influence of lattice change also calculated by DFT. The adsorption energies for O_2 are increased with the change of lattice (Figure 4C), which again demonstrates that the vacancy structure can enhance the performance of ORR.

The v-PdCuCo-AS reported here show excellent electrochemical activity towards ORR. Owing to the vacancies sites on the exterior surface and the Co-embedded, the polarized electronic structures of the v-PdCuCo-AS can effectively promote the charge transfer in the processes of ORR. The MA toward the ORR (at 0.9 V vs. RHE) is found to be 15.55 times that of a commercial Pd/C catalyst and 3.34 times that of the PdCu-AS (0.053 A/mg), respectively. In the case of high surface-to-volume ratio AS, the v-PdCuCo-AS not only exhibits substantial enhancement in mass activity towards ORR, but also retains better durability. Together, our studies show an attractive strategy by engineering the surface structure of the Pd-based-AS nanocatalysts, which are possible to achieve a randomly scattered distribution of vacancy defects on the surface of the catalysts.

Experiment Section

1. Chemicals and materials

Hexadecyltrimethylammonium bromide (CTAB, 99%), Pd/C (20% Pd) were purchased from Sigma-Aldrich. Sodium tetrachloropalladate (II), Potassium Bromide, Ascorbic Acid (AA), Copper (II) nitrate trihydrate, perchloric acid ($HClO_4$, 70%) were supplied by Sinopharm Chemical Reagent Co., Ltd. All the chemicals were of analytical reagent and the ultrapure water in this experiments was with a conductivity of 18.25 MΩ cm.

2. **Preparation of PdCu-AS**

6 mg Na_2PdCl_4, 1.62 mg $Cu(NO_3)_2$, 50 mg KBr, 100 mg CTAB, 90 mg AA were added in sequence into a reaction bottle with 5 mL H_2O at 30℃ under constant magnetic stirring until the mixture well blended. Nitrogen was blown through the bottle to remove oxygen from the system. To obtain well-defined PdCu-AS catalyst, the system was heated up to 90 ℃ and kept for 90 min under the blow of nitrogen. After centrifugation/wash with ethanol, the final

products were obtained.

3. **Synthesis of v-PdCuCo-AS**

6 mg Na_2PdCl_6, 1.62 mg $Cu(NO_3)_2$, 50 mg KBr, 100 mg CTAB, 90 mg AA, 0.351 mg $Co(NO_3)_2$ were added in sequence into a reaction bottle with 5 mL H_2O at 30℃ under constant magnetic stirring until the mixture well blended. To obtain well-defined v-PdCuCo-AS catalyst, the system was heated up to 90 ℃ and kept for 120 min to remove the Co atoms under the blow of nitrogen. After a centrifugation/wash cycle, the v-PdCuCo-AS catalysts were obtained.

4. **Structural and compositional analyses**

High-angle annular dark-field scanning TEM (HAADF-STEM) and energy dispersive X-ray (EDX) mapping analyses were performed using a JEM-ARM200F (JEOL) with an aberration corrector operated at 200 kV. The high-resolution transmission electron microscopy (HRTEM) measurements were conducted on a JEM-2010FEF at an accelerating voltage of 200 kV. Low-magnification Transmission electron microscopy (TEM) measurements were made on a HITACHI H-7650 transmission electron microscope at an acceleration voltage of 80 kV. The compositions of the Pd-based catalysts were determined by ICP–MS (NexION 300Q, PerkinElmer). The XRD analysis was carried out on a Bruker D8 Advance X-ray diffractometer with Cu Kα radiation. The XPS analysis was measured by a Thermo VG Multilab 2000 spectrometer with a monochromatic Al Kα radiation source at room temperature. The XAFS experiments and data processing were performed at the 4W1A-X in Beijing Synchrotron Radiation Facility. The data fitting was done by Artemis program in IFEFFIT.

5. **Electrocatalytic measurements**

The ORR tests were carried out in 0.1 M $HClO_4$ at room temperature through the Pine electrochemistry station using a glassy-carbon Rotating Disk Electrode (RDE, diameter: 5 mm, area: 0.196 cm^2) as the working electrode to load a thin catalyst film. The intact Ag/AgCl (3M KCl) was used as reference electrode and a Pt nanowire was the counter electrode. The concentrations of metal Pd was measured by ICP-MS and the loading amounts of Pd for v-PdCuCo-AS and PdCu-AS, and the commercial Pd/C (JM) catalysts were calculated as 0.046, 0.059, 0.15 mg Pd per cm^2, respectively. The ECSAs of the catalysts were determined by integrating the hydrogen adsorption charge on CVs, which tested in N_2-saturated 0.1 M $HClO_4$ solution with the scan rate of 50 mV/s. The ORR tests were conducted in O_2-saturated 0.1 M $HClO_4$ with the scan and rotation rates of 10 mV/s and 1600 rpm, respectively. The accelerated durability tests (ADTs) for the catalysts were performed in 0.1 M $HClO_4$ with the

sweeping potential from 0.6 V to 1.1 V vs. RHE at a sweep rate of 0.1 V/s for 4000 cycles. The ORR tests in alkaline were performed at room temperature in 0.1 M KOH with the same scan and rotation rates. The methanol oxidation reaction (MOR) and ethanol oxidation reaction (EOR) measurements were conducted in 1 M KOH + 01 M CH_3OH or 1 M KOH + 1 M CH_3CH_2OH solution at room temperature. The scan rate for MOR and EOR tests was at 50 mVs^{-1}. The chronoamperometry was employed to investigate the stability of the catalysts. For HER, all the electrochemical measurements were performed in a three-electrode system in 0.5 M H_2SO_4 electrolyte. To prepare the working electrode, the catalysts were incorporated onto carbon black (Vulcan XC-72) and dispersed ultrasonically in Nafion (0.05 wt %) isopropyl alcohol solution to form an ink. The compositions of the ink were determined by inductively coupled plasma-optical emission spectroscopy (ICP-OES). Then the ink was pipetted onto a glassy carbon electrode (GCE) as a working electrode and the graphite rod was chosed as the counter electrode. The loading amounts of the three catalysts were 10 $\mu g/cm^2$.

6. Calculation methods

It is well known that the chemical reaction sites are almost on materials surfaces. Therefore, we built surface models of PdCu-based structures (including PdCu and Co-doped PdCu) with a vacuum space of 15 Å. And based on these models, we attempted to understand the relationship between the structure and ORR performance of the Co-PdCu by using density functional theory (DFT) calculations. And in present work, all calculations were performed by using the Vienna *Ab initio* Simulation Package (VASP).[53] The ion-electron interactions are described by the projected augmented wave method combined with exchange-correlation functional of Perdew-Burke-Ernzerhof within the generalized gradient approximation.[54,55] For each numerical convergence, the thresholds of 10^{-5} eV in energy and 10^{-2} eV/Å in force under a considerable cutoff energy of 500 eV can be accepted. Grimme DFT-D2 dispersion correction method[56] were employed to describe the weak interactions of O_2 on models. The binding energies (E_b) of O_2 on PdCu-based structures were obtained by the equation, $E_b = E_{Ad} - E_{PdCu} - E_{O2}$, where E_{Ad}, E_{PdCu}, and E_{O2} represent the total energies of O_2 adsorbed PdCu based structures, PdCu based structures, and O_2, respectively. The deformation charge density (ρ_d) describes the charge difference between atoms and compounds, and it was calculated by $\rho_d = \rho_{scf} - \rho_{atom}$, where ρ_{scf} and ρ_{atom} are the charge density of selected compound and the charge densities of all atoms in whole system, respectively, which are performed by VESTA code.[57]

Supporting Information

Supporting Information is available from the Wiley Online Library or from the author.

Acknowledgements
Y. Z. and D. R. contributed equally to this work. The syntheses were supported by National Key R & D Program (2016YFD0500706), National Natural Science Foundation of China (21375043), Research Grant Council of Hong Kong (Grant No: PolyU 152145/15E) and Hong Kong Polytechnic University (Grant No: 1-BBA3, 1-ZVK1 and 1-ZVGH). while the computations were supported by Natural Science Foundation of Jiangsu Province (Grant Numbers: BK20140526).

Received: ((will be filled in by the editorial staff))
Revised: ((will be filled in by the editorial staff))
Published online: ((will be filled in by the editorial staff))

References

[1] H. A. Gasteiger, S. S. Kocha, B. Sompalli, F. T. Wagner, *Appl. Catal. B Environ.* **2005**, *56*, 9.

[2] M. K. Debe, *Nature* **2012**, *486*, 43.

[3] T. H. Wesley, R. Marcel, A. S. Kelsey, G. Alexis, S. Jin, S. H. Yang, *Energy Environ. Sci.* **2015**, *8*, 1404.

[4] D. Yan, Y. Li, J. Huo, R. Chen, L. Dai, S. Wang, *Adv. Mater.* **2017**, *1606459*, 1–20.

[5] J. Staszak-Jirkovský, C.-D. Malliakas, P.-P. Lopes, N. Danilovic, S.-S. Kota, K.-C. Chang, B. Genorio, D. Strmcnik, V.-R. Stamenkovic, M.-G. Kanatzidis, N.-M. Markovic, *Nat. Mater.* **2016**, *15*, 197.

[6] C. Chen, Y. Kang, Z. Huo, Z. Zhu, W. Huang, H. Xin, J. Snyder, D. Li, J. Herron, M. Mavrikakis, M. Chi, K. L. More, Y. D. Li, N. M. Markovic, G. A. Somorjai, P. D. Yang, V. R. Stamenkovic, *Science* **2014**, *343*, 1339.

[7] Y. Zuo, K. Cai, L. Wu, T. Li, Z. Lv, H. Han, *J. Mater. Chem. A* **2015**, *3*, 1388.

[8] G. J. Leong, M. C. Schulze, M. B. Strand, D. Maloney, *Appl. Organomet. Chem.* **2014**, *28*, 1.

[9] Y. Xia, *Angew. Chem. Int. Ed.* **2009**, *48*, 60.

[10] R. A. Martinez-Rodriguez, F. J. Vidal-Iglesias, J. Solla-Gullon, C. R. Cabrera, J. M. Feliu, *J. Am. Chem. Soc.* **2014**, *136*, 1280.

[11] M. Gong, G. Fu, T. Lu, *ACS Appl. Mater. Interfaces* **2014**, *6*, 7301.

[12] Y. Wang, S. Choi, X. Zhao, S. Xie, H. Peng, M. Chi, C. Huang, Y. Xia, *Adv. Funct. Mater.* **2014**, *24*, 131

[13] K. Jiang, P. Wang, S. Guo, X. Zhang, X. Shen, G. Lu, D. Su, X. Huang, *Angew. Chem. Int. Ed.* **2016**, *55*, 1.

[14] S. Gao, Y. Lin, X. Jiao, Y. Sun, Q. Luo, W. Zhang, D. Li, J. Yang, Y. Xie, *Nature* **2016**, *529*, 68.

[15] J. Xie, H. Zhang, S. Li, R. Wang, X. Sun, M. Zhou, J. Zhou, X. W. Lou, Y. Xie, *Adv. Mater*. **2013**, *25*, 5807.

[16] F. Cheng, J. Shen, B. Peng, Y. Pan, Z. Tao, J. Chen, *Nat. Chem.* **2011**, *3*, 79.

[17] A. Shen, Y. Zou, Q. Wang, R. A. Dryfe, X. Huang, S. Dou, L. Dai, S. Wang, *Angew. Chem. Int. Ed.* **2014**, *53*, 10804.

[18] H. Li, C. Tsai, A. L. Koh, L. Cai, A. W. Contryman, A. H. Fragapane, J. Zhao, H. Han, H. C. Manoharan, F. Abild-Pedersen, J. K. Nørskov, X. Zheng, *Nat. Mater.* **2016**, *15*, 48.

[19] L. Dai, Y. Xue, L. Qu, H. J. Choi, J. B. Baek, *Chem. Rev*. **2015**, *115*, 4823.

[20] Y. Nie, L. Li, Z. Wei, *Chem. Soc. Rev.* **2015**, *44*, 2168.

[21] X. Huang, Z. Zhao, L. Cao, Y. Chen, E. Zhu, Z. Lin, M. Li, A. Yan, A. Zettl, M. Wang, X. Duan, T. Mueller, Y. Huang, *Science* **2015**, *348*, 1230.

[22] Y. Wang, N. Zhao, B. Fang, H. Li, X. Bi, H. Wang, *Chem. Rev.* **2015**, *115*, 3433.

[23] M. Shao, Q. Chang, J. P. Dodelet, R. Chenitz, *Chem. Rev.* **2016**, *116*, 3594.

[24] S. Bai, Q. Shao, P. Wang, Q. Dai, X. Wang, X. Huang, *J. Am. Chem. Soc.* **2017**, *139*, 6827.

[25] J. Liu, K. He, W. Wu, T. Song, and M.-G. Kanatzidis, *J. Am. Chem. Soc.* **2017**, *139*, 2900.

[26] S. Ma, H. Li, B. Hu, X. Cheng, Q. Fu, S. Yu, *J. Am. Chem. Soc.* **2017**, *139*, 5890.

[27] H. Li, Q. Fu, L. Xu, S. Ma, Y. Zheng, X. Liu, S. Yu, *Energy Environ.Sci.* DOI: 10.1039/c7ee00573c.

[28] H. Wang, S. Xu, C. Tsai, Y. Li, C. Liu, J. Zhao, Y. Liu, H. Yuan, F. Abild-Pedersen, F. B. Prinz, J. K. Nørskov, Y. Cui, *Science* **2016**, *354*, 1031.

[29] L. Bu, N. Zhang, S. Guo, X. Zhang, J. Li, J. Yao, T. Wu, G. Lu, J. Ma, D. Su, X. Huang, *Science* **2016**, *354*, 1410.

[30] Y. Zuo, L. Wu, K. Cai, T. Li, W. Yin, D. Li, N. Li, J. Liu, H. Han, *ACS Appl. Mater. Interfaces* **2015**, *7*, 17725.

[31] E. Ye, M.-D. Regulacio, S.-Y. Zhang, X. Jun and M.-Y. Han, *Chem. Soc. Rev.* **2015**, *44*, 6001.

[32] Z. Fan, H. Zhang, *Chem. Soc. Rev*. **2016**, *45*, 63.

[33] W. Chen, R. Yu, L. Li, A. Wang, Q. Peng, Y. Li, *Angew. Chem. Int. Ed*. **2010**, *49*, 2917.

[34] C. Xu, Y. Liu, J. Wang, H. Geng, H. Qiu, *J. Power Sources* **2012**, *199*, 124.

[35] C. Xu, A. Liu, H. Qiu, Y. Liu, *Electrochem. Commun.* **2011**, *13*, 766.

[36] D. Wang, H. L. Xin, H. Wang, Y. Yu, E. Rus, D. Muller, F. J. DiSalvo, H. D. Abruña, *Chem. Mater.* **2012**, *24*, 2274.

[37] Y. Wu, C. Wang, L. Zou, Q. Huang, H. Yang, *J. Electroanal. Chem.* **2017**, *789*, 167.

[38] F. Zhu, M. Wang, Y. He, G. Ma, Z. Zhang, X. Wang, *Electrochim. Acta* **2014**, *148*, 291.

[39] M. Jiang, W. Liu, X. Yang, Z. Jiang, T. Yao, S. Wei, X. Peng, *ACS Nano* **2015**, *9*, 10950.

[40] M. Li, Z. Zhao, T. Cheng, A. Fortunelli, C. Chen, R. Yu, Q. Zhang, L. Gu, B. V. Merinov, Z. Lin, E. Zhu, T. Yu, Q. Jia, J. Guo, L. Zhang, W. A. Goddard III, Y. Huang, X. Duan, *Science* **2016**, *354*, 1414.

[41] H. Wang, S. Xu, C. Tsai, Y. Li, C. Liu, J. Zhao, Y. Liu, H. Yuan, F. Abild-Pedersen, F. B. Prinz, J. K. Nørskov, Y. Cui, *Science* **2016**, *354*, 1031.

[42] X. Xia, Y. Wang, A. Ruditskiy, Y. Xia, *Adv. Mater.* **2013**, *25*, 6313.

[43] Z. Peng, H. Yang, *Nano Today* **2009**, *4*, 143.

[44] Y. Xiong, H. Cai, B.-J. Wiley, J. Wang, M.-J. Kim, and Y. Xia, *J. Am. Chem. Soc.* **2007**, *129*, 3665.

[45] Y. Xia, X. Xia, and H.-C. Peng, *J. Am. Chem. Soc.* **2015**, *137*, 7947.

[46] Y. Xiong, Y. Xia, *Adv. Mater.* **2007**, *19*, 3385.

[47] Y. Zuo, T. Li, D. Rao, X. Lei, Q. Li, G. Zhu, R. Lu, H. Han, *J. Phys. Chem. C*, **2016**, *120*, 12305.

[48] G. Wang, B. Huang, L. Xiao, Z. Ren, H. Chen, D. Wang, J. Lu, H. D. Abruña, L. Zhuang, *J. Am. Chem. Soc.* **2014**, *136*, 9643.

[49] L. Ma, C. Wang, M. Gong, L. Liao, R. Long, J. Wang, D. Wu, W. Zhong, M. J. Kim, Y. Chen, Y. Xie and Y. Xiong, *ACS Nano* **2012**, *6*, 9797.

[50] Y. Zuo, T. Li, H. Ren, G. Zhu, K. Han, L. Zhuang, H. Han, *J. Mater. Chem. A* **2016**, *4*, 15169.

[51] J. Hong, Y. Kim, D.-H. Wi, S. Lee, S.-U. Lee, Y.-W. Lee, S. Choi, and S.-W. Han, *Angew. Chem. Int. Ed.* **2016**, *55*, 2753.

[52] S. J. Lee, S. Mukerjee, E. Ticianelli, J. McBreen, *Electrochim. Acta* **1999**, *44*, 3283.

[53] G. Kresse, J. Furthmuller, *Phys. Rev. B* **1996**, *54*, 11169.

[54] P. Blöchl, *Phys. Rev. B* **1994**, *50*, 17953.

[55] G. Kresse, D. Joubert, *Phys. Rev. B* **1999**, *59*, 1758.

[56] G. Stefan, *J. Comput. Chem.* **2006**, *27*, 1787.

[57] M. Koichi, F. Izumi, *J. Appl. Crystallogr.* **2011**, *44*, 1272.

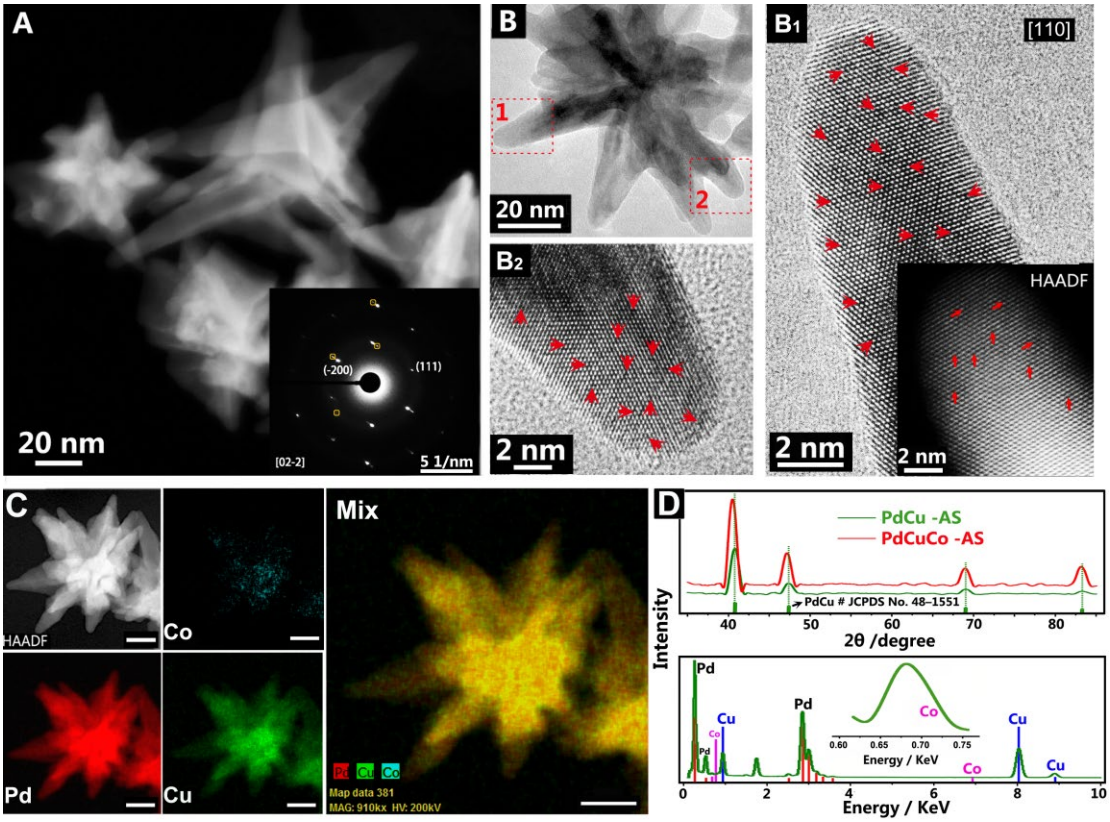

Figure 1. Representative (A) HAADF-STEM (HS) image and the inset is SAED image. (B, $B_{1,2}$) HRTEM images projected along the zone axes of [110] axis and the corresponding bright-field image of a dentritic structure. (C) The typical HS image and the rests are the corresponding STEM-EDS elemental mapping of an individual v-PdCuCo-AS. (D) XRD patterns and TEM-EDX of v-PdCuCo-AS. Scale bars are 20 nm in (C).

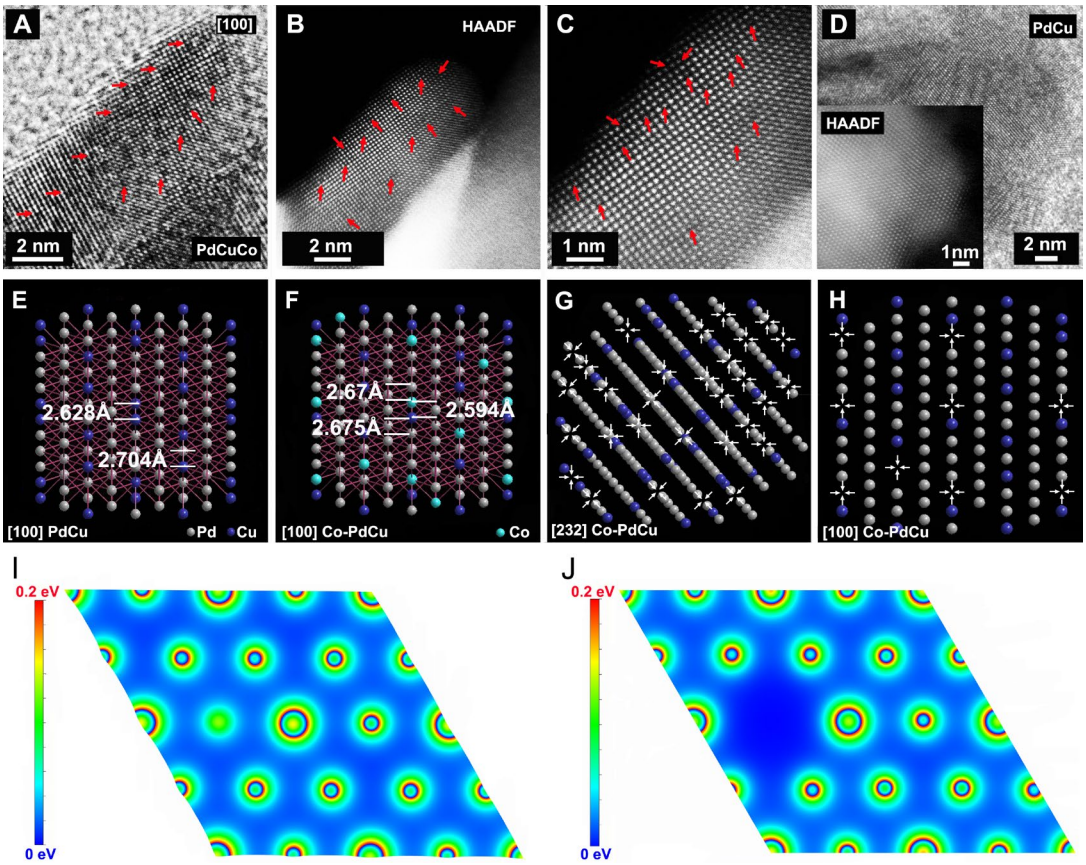

Figure 2. (A) HRTEM image of a typical branch of the PdCuCo-AS from the [100] direction. (B, C) The corresponding enlarged HAADF images. (D) HRTEM image of a typical branch of the PdCu-AS. The inset is the corresponding HRTEM image. (E, F) The approximate PdCu-AS/v-PdCuCo-AS crystal structure from [100] with Pd in grayness, Cu in blue and Co in soft blue and (G, H) the hollow defect sites of the v-PdCuCo-AS from [232] and [100] perspectives view of the crystal structure. (I) The surface charge density of the Co embedded PdCu-AS and (J) the vacancy in v-PdCuCo-AS.

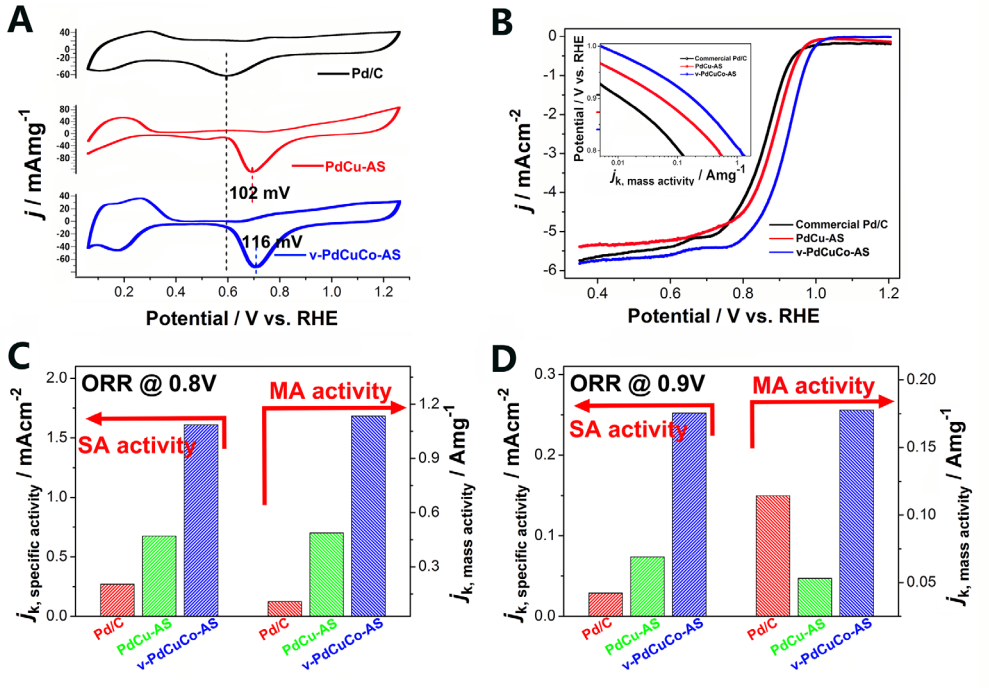

Figure 3. Electrocatalytic properties of commercial Pd/C, PdCu-AS and v-PdCuCo-AS catalysts. (A) The CVs of the catalysts tested in 0.1 M $HClO_4$ solution at room temperature with the sweep rate of 50 mV/s. The ORR polarization curves (B) were recorded in O_2-saturated 0.1 M $HClO_4$ and the inset was the corresponding mass activity Tafel plots for the three catalysts, respectively. Comparison of specific activities and mass activities of the Pd/C, PdCu-AS and v-PdCuCo-AS catalysts at 0.8 V vs. RHE (C) and 0.9 V vs. RHE (D), showing that the v-PdCuCo-AS deliver the enhanced ORR performance of the Pd/C and PdCu-AS catalysts.

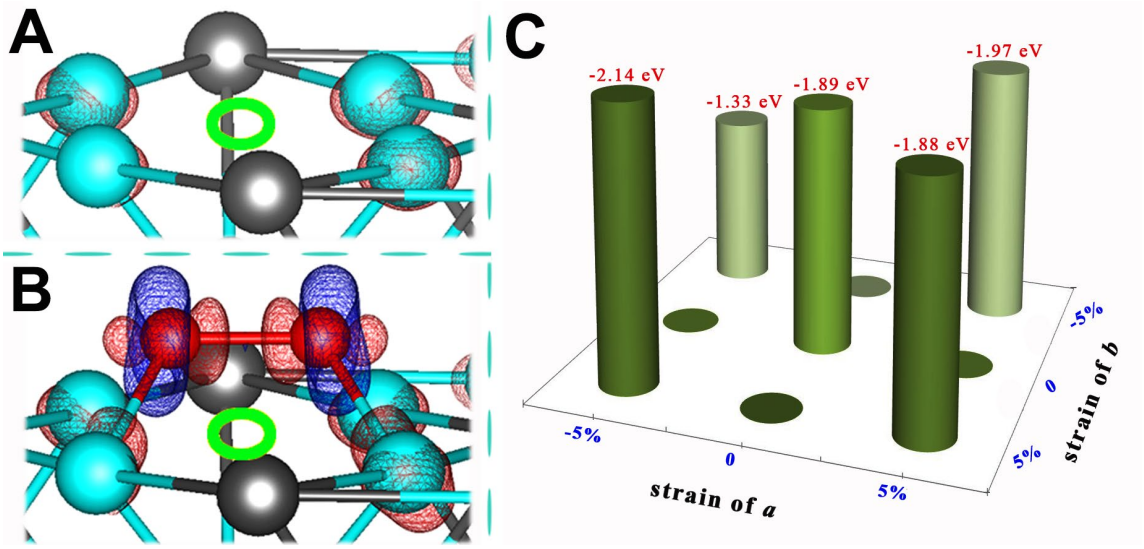

Figure 4. The deformation charge density of (A) the vacancy in v-PdCuCo-AS and (B) O_2 adsorbed v-PdCuCo-AS, (C) the adsorption energies of O_2 on strained v- PdCuCo-AS species. (green ring: vacancy, light blue ball: Cu atom, black ball: Pd atom) (blue area: charge accumulation, red area: charge depletion).

TOC

Structure-engineered Pd-based catalysts at atomic level can effectively improve its catalytic performance. Here we synthesize PdCuCo electrocatalysts with abundant vacancy defects on the exterior surface, which is verified by aberration-corrected transmission electron microscopy. The synergistic effect of the correlated defects and compressive strain effectively improves electro-catalysis activity for the oxygen reduction reaction.

Keywords: PdCuCo alloys, exterior atomic vacancy, compressive strain, oxygen reduction reaction, enhanced electrochemical performance

Atomic vacancies control of Pd-based catalysts with enhanced electrochemical performance

Yunpeng Zuo, Dewei Rao, Shuo Li, Tingting Li, Guilin Zhu, Shuangming Chen, Li Song, Yang Chai, Heyou Han**